Data-Aided Synchronization of Coherent CPM-Receivers

Johannes Huber, *Member, IEEE,* and Weilin Liu, *Student Member, IEEE*

***Abstract*—By means of a signal representation in a signal space spanned by a few time-limited exponential basis-functions, and data-aided maximum-likelihood techniques, novel methods for the joint and nonjoint estimation of carrier-phase and symbol-timing for general coherent CPM receivers are proposed. The estimators are quite simple, especially in obtaining symbol-timing. Simulation results show that synchronizers using such estimation structures exhibit an excellent steady-state behavior. Whereas a fast acquisition of the carrier-phase is always possible, joint synchronizer loops tend to hang-up for CPM-schemes with partial response signaling. Several ways to overcome the hang-up problem are discussed.**

I. Introduction

MODULATION schemes for digital communication systems with constant envelope and continuous phase are intensively discussed in the technical literature, e.g., [1]–[5]. In contrast to more traditional modulation processes, like M-ary phase-shift-keying (M-PSK) or quadrature amplitude modulation (M-QAM), continuous phase modulation (CPM) allows a very efficient amplification of bandlimited signals without a serious reconstruction of spectral sidelobes because the main nonlinear effects of bandpass high-power amplifiers, namely, AM/AM and AM/PM conversion, are avoided. Additionally, the *power efficiency* of CPM increases by the *inherent trellis* code due to the phase continuity condition and the nonlinear intersymbol interference (ISI), which results from the smoothed phase pulses causing phase transients over several symbol intervals (partial-response-signaling). Both of these effects contribute to a reduction of the signal bandwidth and, therefore, CPM is highly *bandwidth efficient* too. However, the practical implementation of coherent CPM receivers proposed in [2]–[5], is rather complex. Especially for $M = 4$ and $M =$ 8-ary schemes with smoothed phase pulses, which offer more power and bandwidth efficiency than binary schemes, this complexity problem seems to be a serious disadvantage of CPM, because simple receiver structures, such as those used for minimum shift keying (MSK) with quadrature or serial demodulation [6], cannot be applied.

In [12] solutions for two complexity problems are proposed by the use of a signal space with reduced dimensionality, which is formed over a few (4 or 6) time-limited sinusoidal functions and the application of reduced state sequence estimation (RSSE, [13], [14]) to CPM.

A third problem of CPM receivers is the synchronization of the symbol-timing and the carrier-phase in the coherent case. The conventional synchronization method using a nonlinear device for the generation of discrete spectral lines [8] cannot successfully be applied to CPM because of the small carrier-to-noise ratio. Loop filters with an extremely small bandwidth would be necessary with which even loose requirements on the dynamic behavior of the synchronizer would be sacrificed. In [9], [10] data-aided synchronization methods are applied to a special CPM scheme, namely, continuous phase frequency shift keying (CPFSK) with multi-h signaling [11]. But efficient synchronizers for general CPM, especially for $M > 2$-ary schemes have not been proposed yet.

In the present paper the results of [12] are used to solve the synchronization problem. In order to improve the readability of the paper, we give a short recapitulation of the signal representation by samples in the frequency domain in Section II. Using a maximum-likelihood approach, structures of data-aided estimators for the carrier-phase and symbol-timing deviations are derived in Section III. We show that a proper choice of the basis functions of the signal space can essentially simplify the synchronization, and both estimations can be performed in a simple way by a single unit. Simulation results show that for CPM schemes with a small denominator of the modulation index, carrier-phase synchronization can be performed very efficiently (Section IV). The degradation due to imperfect carrier-phase synchronization is smaller than for other trellis-coded modulation schemes with comparable power and bandwidth efficiency, especially at a low signal-to-noise ratio (SNR). On the other hand, there are some problems concerning symbol-timing synchronization, when the maximum of the likelihood-function between the received and a reference signal, which corresponds to the tentative decided data, is searched iteratively.

II. Signal Representation by Spectral Samples

Detailed descriptions of CPM may be found in [2]–[5]. The same notation is used as in [12] which is very similar to [2]–[4]. But in contrast to [12] we use here the equivalent complex baseband signal representation.

A CPM signal $s(\boldsymbol{\alpha}, t)$ can be interpreted as a sequence of time-limited signal segments $\rho(\boldsymbol{a}_m, t)$:

$$s(\boldsymbol{\alpha}, t) = \sum_{m=-\infty}^{\infty} \rho(\boldsymbol{a}_m, t - mT). \tag{1}$$

Paper approved by the Editor for Synchronization and Optical Detection of the IEEE Communications Society. Manuscript received January 29, 1990; revised July 27, 1990. This work was supported by the German Research Community (Deutsche Forschungsgemeinschaft DFG) under Contract Tr. 160/5-3. This paper was presented in part at the IEEE GLOBECOM '90, San Diego, CA, December 1990.

J. Huber is with Lehrstuhl fur Nachrichtentechnik, Cauerstr. 7, D-8520 Erlagen, Germany.

W. Liu is with Ascom Tech. Ltd., Baden, Switzerland.

IEEE Log Number 9105159.

with

$$\rho(\boldsymbol{a}, t) = 0 \quad \text{for } t \notin [0, T).$$

All different signal segments which can appear within one modulation interval T, form the signal set of a CPM scheme. The particular signal element $\rho(\boldsymbol{a}_m, t - mT)$ for the time interval $mT \leq t < (m+1)T$ is selected by an address

$$\boldsymbol{a}_m = (\Theta_{m-L}, \alpha_{m-L+1}, \cdots, \alpha_m), \tag{2}$$

which is generated from the data sequence $\boldsymbol{\alpha}$, $\alpha_i \in \{\pm 1, \pm 3, \cdots, \pm(M-1)\}$, by a trellis encoder [12], [16]. This encoder controls the phase continuity (recursive structure) and the smoothing of the phase transients (nonrecursive structure). In (2) L denotes the duration of the slope of the phase pulses in modulation intervals [2]. The phase-state Θ_{m-L} involves the contributions of all past modulator input data α_i; $i \leq m - L$ to the signal phase for which the phase pulses have already achieved a constant value. The correlative vector $(\alpha_{m-L+1}, \cdots, \alpha_m)$ of input data determines the phase transient.

If the carrier frequency is used for the transformation of the CPM signal into an equivalent complex baseband signal, there are at most $2pM^L$ different signal elements and $2pM^{L-1}$ encoder states where p denotes the denominator of the modulation index $h = k/p$. In [12], [16] it is shown that a description with pM^L signal elements and pM^{L-1} states is possible in all cases, if a proper transformation frequency is applied which differs from the carrier frequency.

As samples in the time domain are well suited to represent signals which are limited in bandwidth, samples in the frequency domain are appropriate to describe the time-limited signal elements. In [12] we have shown that the signal elements of almost all CPM schemes which are relevant in practice, can be represented by $D = 2$ or $D = 3$ pairs of time-limited sine and cosine functions with sufficient accuracy. The equivalent low-pass basis-functions of the signal space are D exponential functions of duration T:

$$e^{j2\pi f_d t}, \qquad 0 \leq t < T$$

with

$$f_d = \frac{\Delta f}{2}(2d - 1 - D); \qquad d \in \{1, \cdots, D\}. \tag{3}$$

Thus, the signal elements $\rho(\boldsymbol{a}, t)$ are approximated by

$$\rho(\boldsymbol{a}, t) \approx \sum_{d=1}^{D} \rho_d(\boldsymbol{a}) \cdot e^{j2\pi f_d t}. \tag{4}$$

The signal elements result from a multiplication of the band-limited signal with rectangular windows of length T. Therefore, the magnitudes of their spectra are all similar to $|\sin(\pi fT)/(\pi fT)|$-functions. When orthogonal functions are used, i.e., the frequency spacing parameter is chosen to $\Delta f = 1/T$, the samples in the frequency domain are taken close to the minima of these spectra. Therefore, many terms are necessary in such a series expansion in order to represent the Euclidean distances between the signal elements with sufficient accuracy. Thus, as we desire a small number

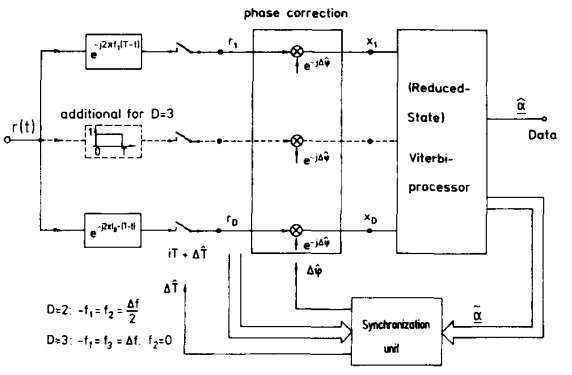

Fig. 1. Block diagram of the coherent CPM receiver with reduced dimensionality (complex baseband representation).

D of complex dimensions, a maximization of the minimum Euclidean distance in almost all cases leads to a nonorthogonal basis with $\Delta f < 1/T$ [12], [17]. Thus, the reference vectors $\boldsymbol{\rho}(\boldsymbol{a}) = (\rho_1(\boldsymbol{a}), \cdots, \rho_D(\boldsymbol{a}))$ have to be calculated by

$$\boldsymbol{\rho}(\boldsymbol{a}) = (\sigma_1(\boldsymbol{a}), \cdots, \sigma_D(\boldsymbol{a})) \cdot \boldsymbol{C}^{-1} \tag{5}$$

from the spectral samples $\sigma_d(\boldsymbol{a})$ at the frequency f_d

$$\sigma_d(\boldsymbol{a}) = \int_0^T \rho(\boldsymbol{a}, t) e^{-j2\pi f_d t}\, dt, \qquad d = 1, \cdots, D, \tag{6}$$

and the inverse of the covariance matrix $\boldsymbol{C}$ of the D exponential basis-functions. For a constant envelope signal and the additive white Gaussian noise channel (AWGN) the correlations of the segment of the receiver-input signal with the signal elements $\rho(\boldsymbol{a}, t)$ are proper branch-metrics (log-likelihood terms) for the (reduced state) sequence estimation procedure. For the mth interval $mT \leq t < (m+1)T$ and using the signal expression (4) these metrics $\lambda(\boldsymbol{a}, m)$ are approximately given by

$$\begin{aligned} \lambda(\boldsymbol{a}, m) &= \mathrm{Re}\left\{ \int_0^T r(t + mT) \rho^*(\boldsymbol{a}, t)\, dt \right\} \\ &\approx \mathrm{Re}\left\{ \sum_{d=1}^{D} r_d(m) \cdot \rho_d^*(\boldsymbol{a}) \right\} \\ &= \mathrm{Re}\{ \boldsymbol{r}(m) \cdot \boldsymbol{\rho}^{*T}(\boldsymbol{a}) \} \end{aligned} \tag{7}$$

with

$$r_d(m) = r_{Id}(m) + j r_{Qd}(m) = \int_0^T r(t + mT) e^{-j2\pi f_d t}\, dt \tag{8}$$

and

$$\boldsymbol{r}(m) = (r_1(m), \cdots, r_D(m)). \tag{9}$$

Fig. 1 shows a block diagram of this receiver with spectral sampling using equivalent baseband signals. If an uncontrolled local carrier oscillator is used for the quadrature demodulation, an estimated phase error $\Delta\hat{\varphi}$ can be corrected in the same way as for M-PSK or M-QAM.

The reader may be astonished at this point why we take samples in the frequency domain, whereas a correlation can also be done with samples in the time domain. Indeed, as long as the sequence estimation is performed by a full state Viterbi algorithm, there is no difference. The same number D of multiply-accumulate operations is necessary for the metric calculations in both dual methods. But since the individual signal segments are not strictly band-limited, performance degradations occur for suboptimal sequence estimation algorithms with state reduction, when only D samples per interval are taken in the time domain [15].

In this context the main reason for a representation of signal elements by spectral samples [cf. (4)] is that derivatives of the signals can be performed in a very simple way. Therefore, simple synchronizers for the symbol-timing can be derived by a maximum-likelihood approach. Spectral samples can be obtained from time samples of the receiver-input signal with sufficient accuracy by a FIR-filter with at most 3-D taps [19].

III. ML–Estimation of the Carrier Phase and Symbol Timing

We assume that the local oscillators for the symbol-clock and the carrier in the coherent receiver have sufficient accuracy and stability, and that the channel varies slowly. Thus, the deviations of the local carrier-phase and the symbol-clock relative to the receiver-input signal vary slowly compared to the symbol rate $1/T$. In the receiver an estimate $s(\hat{\boldsymbol{\alpha}}, t - T_0) \cdot e^{j\varphi_0}$ of the received signal is generated with an estimated data sequence $\hat{\boldsymbol{\alpha}}$, a time deviation T_0 relative to the local symbol-clock, and a phase rotation φ_0 relative to the local carrier-oscillation. For joint maximum-likelihood (ML) estimation [21], [22] the parameters $\hat{\boldsymbol{\alpha}}$, T_0 and φ_0 have to be chosen *jointly* in such way, that the likelihood-function $\lambda(\hat{\boldsymbol{\alpha}}, T_0, \varphi_0)$ for the received signal $r(t)$ achieves its maximum. For a constant envelope signal and the additive white Gaussian noise channel (AWGN) the correlation

$$\lambda(\hat{\boldsymbol{\alpha}}, T_0, \varphi_0) = \mathrm{Re}\left\{ e^{-j\varphi_0} \int_{-\infty}^{+\infty} r(t) s^*(\hat{\boldsymbol{\alpha}}, t - T_0)\, dt \right\} \quad (10)$$

is such a likelihood function [5]. Because of the assumed quite different dynamic behavior of the data sequence, and the carrier-phase and symbol-clock deviations, the search for the maximum is usually split into a sequence estimation process for which a perfect estimation of T_0 and φ_0 is assumed (coherent receiver), and a *data-aided synchronization* for which perfect symbol decisions are assumed. Often, it is more favorable for the synchronization to use preliminary, tentative decisions, here denoted by $\tilde{\boldsymbol{\alpha}}$ because an increased error rate of this sequence causes less degradation than the delay of the MLSE or RSSE process, as synchronizer loops with a long delay tend to be unstable. Additionally, a weight-function $w_c(t)$ should be introduced into (10) in order to attenuate the signal for times far in the past, as meanwhile the carrier-phase and the symbol-clock may have been altered due to the frequency offsets of the local oscillators or channel variations. Taking the weighted average up to the actual m-th interval, a modified synchronizer likelihood-function is defined by

$$\lambda(m, T_0, \varphi_0) = \mathrm{Re}\{ e^{-j\varphi_0} Z(m, T_0) \} \quad (11)$$

with the complex correlation

$$Z(m, T_0) = \int_{-\infty}^{(m+1)T+T_0} w_c[(m+1)T + T_0 - t] \cdot r(t) s^*(\tilde{\boldsymbol{\alpha}}, t - T_0)\, dt. \quad (12)$$

For time-variant channels the optimization of the weight-function $w_c(t)$ or its discrete time version $w(i)$ may be implemented by a Kalman filter [23]. Different filters $w_\varphi(i)$ and $w_T(i)$ may be necessary for the carrier-phase and symbol-timing synchronization according to the different dynamic behavior of these processes.

While a carrier-phase shift φ_0 simply corresponds to a rotation of the complex correlation $Z(m, T_0)$ [cf. (11)], an implementation of a variable time shift T_0 is more difficult. For the calculation of $Z(m, T_0)$ by discrete time correlation, the samples of a time shifted version $s(\tilde{\boldsymbol{\alpha}}, t - T_0)$ of the reference signal have to be calculated by interpolation and resampling.

For the signal representation by spectral samples and the use of a discrete time weight function $w(i)$ we separate (12) into:

$$Z(m, T_0) = \sum_{i=-\infty}^{m} w(m-i) \int_{T_0}^{T+T_0} r(t + iT) \cdot \rho^*(\tilde{\boldsymbol{a}}_i, t - T_0)\, dt. \quad (13)$$

If we restrict the clock deviation T_0 to be small, i.e., $T_0 \ll T$, the shift in the limits of the integral in (13) may be ignored. This assumption is valid for the steady-state timing error, which is small when the local clock generator (VCC: voltage controlled clock) is controlled by estimates $\Delta\hat{T}(m)$ of the clock deviation. Under this approximation, an insertion of (4) into (13) yields:

$$Z(m, T_0) \approx \sum_{i=-\infty}^{m} w(m-i) \sum_{d=1}^{D} \rho_d^*(\tilde{\boldsymbol{a}}_i) \cdot e^{j2\pi f_d T_0} \int_0^T r(t + iT) e^{-j2\pi f_d t}\, dt. \quad (14)$$

Replacing the integral by (8) and letting

$$Z_d(m) = \sum_{i=-\infty}^{m} w(m-i) \cdot \rho_d^*(\tilde{\boldsymbol{a}}_i) \cdot r_d(i) \quad (15)$$

we obtain

$$Z(m, T_0) \approx \sum_{d=1}^{D} Z_d(m) \cdot e^{j2\pi f_d T_0}. \quad (16)$$

Thus, a small time shift T_0 is approximated by phase shifts for the components of the complex correlation.

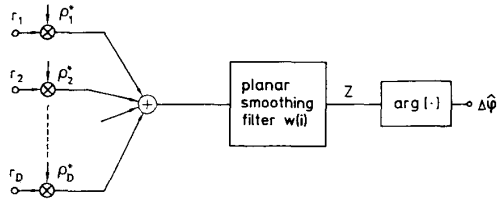

Fig. 2. Data-aided ML-estimator of the carrier-phase deviation ($T_0 = 0$) with planar smoothing filter $w(i)$ [signal representation by spectral samples].

A. ML-Carrier Phase Estimation

Assuming that both the data sequence $\hat{\boldsymbol{\alpha}}$ and the symbol-clock shift T_0 are known, the likelihood function (11) achieves the maximum at the carrier-phase difference φ_0, by which the complex number $Z(m, T_0)$ is rotated towards the positive real axis of the complex plane [22]. Therefore,

$$\Delta\hat{\varphi}(m) = \arg[Z(m, T_0)] \tag{17}$$

where

$$\arg[z] = \tan^{-1}\left(\frac{\mathrm{Im}\{z\}}{\mathrm{Re}\{z\}}\right) + \frac{\pi}{2}[1 - \mathrm{sign}(\mathrm{Re}\{z\})] \tag{18}$$

is a ML-estimate of the difference of the phase of the local carrier-oscillation relative to the receiver input signal. Fig. 2 shows a block diagram of the ML-estimator of the carrier-phase deviation for a signal representation by spectral samples ($T_0 = 0$). A time shift $T_0 \neq 0$ can be taken into account by a simple phase rotation of the components (16). The weight-function $w(i)$ is discrete time filter for a complex signal (so-called planar filter). This carrier-phase estimation for a signal space with $D > 1$ complex dimensions per interval is a straight forward extension of the solution derived in [24] for linear modulation.

The ML-estimate $\Delta\hat{\varphi}(m)$ can be used directly to correct the phase error of the vector $\boldsymbol{r}(m)$ via the phase rotation unit (Fig. 1):

$$\boldsymbol{x}(m) = \boldsymbol{r}(m)e^{-j\Delta\varphi(m)}. \tag{19}$$

But $\Delta\hat{\varphi}(m)$ can also be used to control the local carrier-oscillator (VCO). In this case the phase error is minimized in an adaptive approach.

B. ML-Symbol Timing Estimation

For a ML-estimation $\Delta\hat{T}(m)$ of the deviation of the local symbol-clock relative to the receiver-input signal, we have to determine T_0 in such way that (11) achieves its maximum for a given data sequence $\hat{\boldsymbol{\alpha}}$ and a fixed carrier-phase offset φ_0. In order to determine the maximum of (11), we use (16) and calculate the derivative:

$$\frac{d\lambda(m, T_0, \varphi_0)}{dT_0} = \mathrm{Re}\left\{\sum_{d=1}^{D} j2\pi f_d Z_d(m)e^{-j\varphi_0} \cdot e^{j2\pi f_d T_0}\right\} = 0. \tag{20}$$

In general the roots of this equation cannot be expressed analytically. But for the cases $D = 2$ with $f_1 = -f_D$, and $D = 3$ with $f_1 = -f_D$ and $f_2 = 0$ [cf. (3)], which are important in practice [12], the explicit solution can simply be derived. For this we apply $\mathrm{Re}\{jz\} = -\mathrm{Im}\{z\}$, cancel the constant $-2\pi f_1$ in (20), and use the abbreviation

$$X_d(m) = Z_d(m) \cdot e^{-j\varphi_0}. \tag{21}$$

The components $X_d(m)$ correspond to the correlation (15) but using $x_d(m)$ instead of $\boldsymbol{r}_d(m)$ [cf. (19) and Fig. 1]. By this we get from (20)

$$\mathrm{Im}\{X_1(m)e^{j2\pi f_1 T_0} - X_D(m)e^{-j2\pi f_1 T_0}\} = \mathrm{Im}\{[X_1(m) + X_D^*(m)]e^{j2\pi f_1 T_0}\} = 0. \tag{22}$$

Thus, the ML-estimate of the symbol-clock deviation relative to the receiver-input signal is given by

$$\Delta\hat{T}(m) = \frac{1}{\pi\Delta f(D-1)} \arg[X_1(m) + X_D^*(m)] \quad D = 2 \text{ or } D = 3. \tag{23}$$

[Please note that $f_1 < 0$, cf. (3)]. A short examination of (11) shows that (23) is the unique solution which always corresponds to the maximum of the likelihood function, whereas the second root of (22) $2\pi f_1 T_0 = \pi - \arg[X_1(m) + X_D^*(m)]$ leads to the minimum (see also [26]). Fig. 3 shows the structure of the proposed estimator. Again a discrete time planar smoothing filter is applied. The signal representation using time-limited exponential basis-functions transforms small time shifts T_o into phase shifts $\varphi_d = 2\pi f_d T_o$ of the components $Z_d(m)$ of the complex correlation (16). This may be interpreted simply by the fact, that a time shift causes an increasing phase shift in the frequency domain. Therefore, the estimator of the symbol-clock deviation differs from the carrier-phase estimator in Fig. 2 only in the conjugate of $Z_D(m)$ and an omission of the dc-component for $D = 3$, which clearly contains no timing information. The signal representation by spectral samples offers the following advantages for the ML symbol-clock synchronization.

1) No equipment is necessary to generate the derivative (20) of the likelihood-function [5], [18].
2) As the timing estimation is referred to a special form of phase estimation, a simple common estimator for the carrier phase and symbol timing exists.
3) In contrast to other methods of a signal representation, an *explicit* solution exists for the maximum of the approximate likelihood-functions if $D \leq 3$. Therefore, one vector $\boldsymbol{r}(m)$ per interval is sufficient to perform a ML-estimation, i.e., no form of multiple probes, interpolation, "oversampling," or parallel processing for several clock shifts is necessary to implement the symbol-clock synchronizer in a discrete time digital receiver.

The estimate $\Delta\hat{T}(m)$ will normally be used to control the local VCC in order to minimize the timing error in an adaptive approach. But the control of a time shift of the receiver input signal, which may be performed by an interpolation unit in a time discrete digital receiver, also is possible.

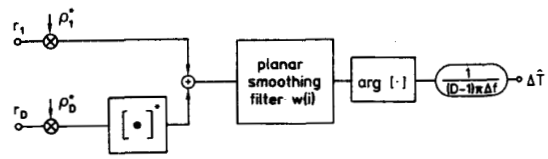

Fig. 3. Data-aided ML-estimator of the symbol-clock deviation ($\varphi_0 = 0$) for $D = 2$ and $D = 3$.

C. Joint ML-Estimation of Carrier-Phase and Symbol-Timing

From (11) it is obvious, that the likelihood function achieves its maximum for a given data sequence $\tilde{\alpha}$ for that time shift T_o, which maximizes the magnitude of $Z(m, T_o)$, and that phase shift φ_0 which rotates this complex number towards the real axis [21], [22].

Unfortunately, an explicit solution for the joint maximum of the likelihood-function can be given only for the special but important case $D = 2$. For $D \geq 3$ near optimum explicit solutions can be derived. For $D = 2$, the magnitude of $Z(m, T_o)$ is [$f_1 = -f_2 = -\Delta f/2$, cf. (3), (16)]:

$$|Z(m,T_0)| = \left|Z_1(m)e^{-j\pi\Delta f T_0} + Z_2(m)e^{j\pi\Delta f T_0}\right|$$
$$= \Big||Z_1(m)|e^{j(\arg(Z_1(m))-\pi\Delta f T_0)} + |Z_2(m)|e^{j(\arg(Z_2(m))+\pi\Delta f T_0}\Big|. \quad (24)$$

For two complex numbers, say Y_1 and Y_2, the inequality $|Y_1 + Y_2| \leq |Y_1| + |Y_2|$ holds with equality if and only if $\arg[Y_1] = \arg[Y_2]$. Therefore, the joint ML-estimate of the deviation of the local symbol-clock relative to the received signal is

$$\Delta\hat{T}(m) = \frac{\arg[Z_1(m)] - \arg[Z_2(m)]}{2\pi\Delta f}. \quad (25)$$

Inserting (25) into (16) the angle of the complex correlation $Z(m, \Delta\hat{T}(m))$ with maximum magnitude is forced to be the arithmetic mean of the angles of its components. Therefore, the joint ML-estimate of the phase deviation of local carrier-oscillation is

$$\Delta\hat{\varphi}(m) = \frac{1}{2}(\arg[Z_1(m)] + \arg[Z_2(m)]). \quad (26)$$

Equations (25), (26) may be interpreted by the facts, that a carrier-phase error causes identical phase rotations of each exponential basis-function, whereas a timing error corresponds to a delay and, therefore, causes opposite phase shifts [cf. (16) and Fig. 4]. The mutual influence of a timing error on the carrier-phase estimation or vice versa is completely eliminated by this joint estimator. This property makes the synchronizer very robust for time-variant channels.

Fig. 5 shows the joint estimator which causes almost no additional equipment compared to the specific estimators in Figs. 2 and 3. Therefore, this joint estimator not only is attractive due to its performance (Section IV), but also due to its low complexity.

For the receiver using $D = 3$ complex dimensions per interval (receiver with six real dimensions [12]) no simple optimum joint estimator exists. But when the average in (15) is taken over a sufficient number of intervals, we can expect that the magnitudes $|Z_1(m)|$ and $|Z_3(m)|$ are approximately equal. Additionally, we know from (16) that a symbol clock shift causes opposite phase shifts in these components. Therefore, the estimates

$$\Delta\hat{T}(m) = \frac{\arg[Z_1(m)] - \arg[Z_3(m)]}{4\pi\Delta f} \quad (27)$$

$$\Delta\hat{\varphi}(m) = \frac{1}{3}\{\arg[Z_1(m)] + \arg[Z_2(m)] + \arg[Z_3(m)]\} \quad (28)$$

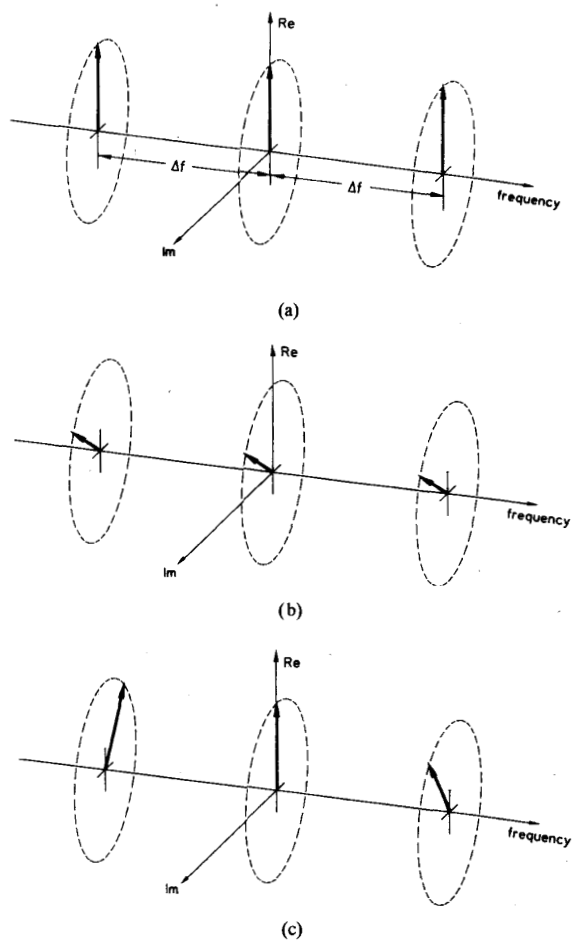

Fig. 4. Illustration of phase shifts of the basis-functions of the signal space; (a) perfect synchronization, (b) carrier-phase offset $\Delta\varphi$, (c) symbol-clock offset ΔT.

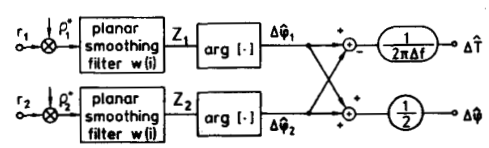

Fig. 5. Joint data-aided ML-estimators of the carrier-phase and the symbol-clock deviations ($D = 2$).

are good approximations of the joint ML-estimation for $D = 3$.

D. Additional Remarks

In [12], [17] it is shown, that there is a wide range of the frequency spacing parameter Δf [see (3)] where the SNR performance losses for the sequence estimation are very small. In order to minimize the variance of the timing estimation the maximum value Δf within this range should be chosen, [cf. (23), (25), (27)]. Note that the proposed generation of a control-signal for the symbol-timing synchronization by means of data-aided phase estimations is only possible for receivers implementing a signal representation in a multidimensional space per interval.

The conventional joint data-aided synchronization [18], [25] uses the partial derivatives of the likelihood function (11)

$$\left.\frac{\partial\lambda(m,T_0,\varphi_0)}{\partial\varphi_0}\right|_{\varphi_0=T_0=0} = \sum_{d=1}^{D} \mathrm{Im}\{Z_d(m)\} \qquad (29)$$

and

$$\left.\frac{\partial\lambda(m,T_0,\varphi_0)}{\partial T_0}\right|_{\varphi_0=T_0=0} = -2\pi\sum_{d=1}^{D} f_d\ \mathrm{Im}\{Z_d(m)\} \qquad (30)$$

to control the local VCO and VCC (cf. also [9], [10]). For a small carrier-phase error $\Delta\varphi$ and a small clock-shift ΔT the term $\mathrm{Im}\{Z_d(m)\} \approx |Z_d(m)| \cdot \Delta\varphi_d(m)$ may be interpreted as an estimate of the phase difference $\Delta\varphi_d(m)$ of the dth basis-function weighted by the energy of the signal represented by this dth complex dimension. Therefore, (29) and (30) are weighted estimates of $\Delta\varphi$ and ΔT for each interval followed by smoothing filters. This approach claims less hardware, but offers less noise attenuation than the estimators using planar filters.

For small steady-state residual timing and phase errors the nonjoint solutions A and B produce independent estimations, too. Therefore, the optimum combination of the proposed structures has to be chosen according to the actual requirements in practice.

IV. Simulation Results

In order to study both the steady state and acquisition behavior of the proposed synchronizer, a computer program was written for the simulation of CPM schemes with different parameters (M, h, phase pulses) including carrier-phase and symbol-timing synchronization of the receiver. Throughout the simulations the AWGN-channel with a one-sided spectral noise power density N_o is assumed.

The outputs $\Delta\hat{T}(m)$ and $\Delta\hat{\varphi}(m)$ of the estimators were not directly used to correct the symbol-timing and carrier-phase deviations, but as control signals of the VCO and VCC in synchronizer loops (PLL). Thus, the deviations are minimized in an adaptive process. The discrete time planar smoothing filters within the estimators were chosen to be one-pole low-pass filters (PT1). In Fig. 6 linear models of both loops for small differences ΔT and $\Delta\varphi$ are shown. The symbol-timing synchronization is performed by a simple second-order loop

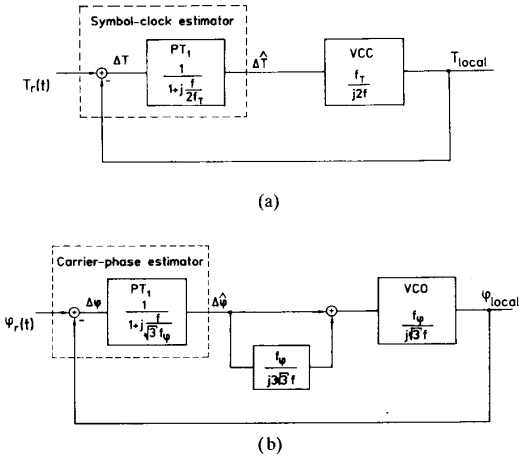

Fig. 6. Block diagram of the synchronizer loops, which are used for simulation; (a) symbol-clock loop. $T_r(t)$: actual phase of the symbol-clock of the receiver-input signal, T_{local}: actual phase of the local clock oscillation. (b) carrier-phase loop. $\varphi_r(t)$: actual carrier-phase of the receiver-input signal, φ_{local}: actual phase of the local carrier oscillation.

(PLL 2) [Fig. 6(a)]. A similar loop is used for the carrier-phase synchronization, but an integrator with a lag-filter is added in order to compensate a possible carrier-frequency offset, [cf. Fig. 6(b)]. In order to obtain a simple model which is characterized by only two parameters, namely the 6 dB cutoff frequencies f_φ and f_T of the respective transfer-functions of these linear models, both loops were designed according to the aperiodic limiting case [Fig. 6(a) and (b)]. The results are given for the combination of the nonjoint carrier-phase estimation (17) (Fig. 2) together with the joint structure (25), (27) [Fig. 5] for the symbol timing.

The data on the top of the FIFO path register of that path in the trellis, which actually has the best metric, are fed back to the data-aided estimators without any decision delay.

Here results are given for a quaternary CPM scheme ($M = 4$) with smoothed phase pulses of the type raised cosine over $L = 3$ intervals, and modulation index $h = 1/2$ (cf. [2]–[4]). This scheme offers an interesting comparison of CPM with octal PSK combined with a rate 2/3 four state trellis-encoder (TC8PSK), as both schemes have almost the same coding-gain and signal bandwidth. Additionally, a RSSE-procedure for this CPM scheme requires 4 states, too [12]. The CPM scheme offers the advantage of a constant envelope of the band-limited signal.

A. Carrier-Phase Synchronization

Fig. 7 shows simulation results which were obtained assuming steady-state synchronizer conditions. In Fig. 7(a) rms-values of the variations of the local carrier-phase are given for several loop bandwidths and signal to noise ratios (SNR) E_b/N_0 (E_b: equivalent bit energy). In Fig. 7(b) the corresponding simulated bit error rates (BER) are shown. The results demonstrate that a stable data-aided carrier-phase synchronization is even possible at a low SNR and a high loop bandwidth. Only for $f_\varphi = 1/(20T)$ phase-skips between both

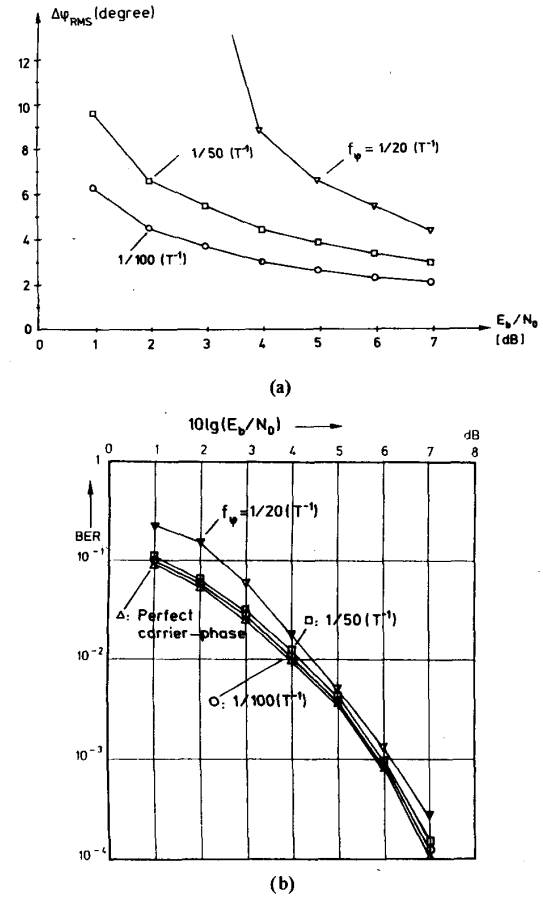

Fig. 7. Simulation results for the carrier-phase synchronization with different loop bandwidths f_φ and perfect symbol-clock ($M = 4$, $h = 1/2$, 3RC, $D = 3$, reduced-state sequence estimation (RSSE) with 8 states); (a) rms phase deviation, (b) Bit Error Rates (BER).

stable points (0° and 180°) often occur for $E_b/N_o < 4$ dB; here imperfect synchronization causes an increased error rate.

In Fig. 8, an example of the acquisition of the carrier-phase from an initial worst case position is shown. A stable position is reached after a small number of intervals in the most direct way.

The results of Figs. 7 and 8 and of many further tests for several CPM schemes with different parameters prove that data-aided carrier-phase synchronization of coherent CPM receivers works without any problems. The degradation of the coherent receiver due to imperfect carrier phase synchronization is small, because CPM schemes are normally rotationally invariant (mapping of the information to phase-increments, cf. [12]). Additionally, for schemes with a small denominator p of the modulation index h the stable phase points are separated by a large distance. This fact is illustrated in Fig. 9 for the special CPM scheme and 8PSK. Since the signal points are separated along the frequency axis for CPM, the points need not to be arranged as densely on one circle or plane as for trellis-coded PSK or QAM. Therefore, phase-skips which produce long series of errors, occur very rarely for this CPM scheme.

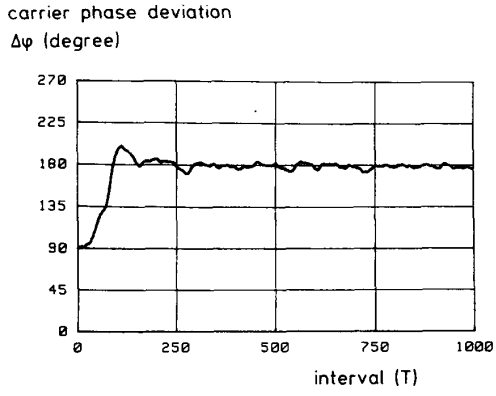

Fig. 8. Example of the acquisition of the carrier-phase from a worst case initial position ($M = 4$, $h = 1/2$, 3RC, $D = 3$, $E_b/N_0 = 5$ dB, loop bandwidth $f_\varphi = 1/(50\ T)$).

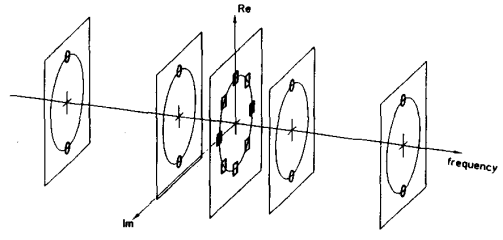

Fig. 9. Illustration of the sensitivity to a carrier-phase error of 8PSK (marked by □) and a CPM scheme ($M = 4$, $h = 1/2$; marked by ○).

The insensitivity of CPM schemes with a small parameter p to imperfect carrier-phase synchronization is a second important advantage of CPM. It makes possible to use CPM efficiently in concatenated coding schemes. In order to utilize the overall high coding-gain of such schemes, the demodulation and synchronization have to be performed at a very low SNR. Due to the small number of nearest neighbor error-events and the insensitivity to imperfect synchronization, CPM is well suited for the bandwidth-efficient inner part of such schemes. In [27] examples for the concatenation of CPM and Reed–Solomon codes with low coding and decoding complexity are given which operate (including synchronization) close to the maximum cutoff-rate R_o of constant envelope schemes (AWGN-channel).

The examples show that the carrier-phase synchronization can also be performed for time-variant channels (e.g., mobile radio) where a great loop bandwidth has to be chosen in order to trace fast phase variations. Especially for such applications the coherent receiver structure together with an optimized (perhaps time-variant) synchronizer should be preferred to noncoherent CPM receivers, which use a sequence-estimation with metrics derived from the magnitude of the complex correlation [4], [28]. Although the carrier-phase is arbitrary, it has to be constant over the whole message for such incoherent receivers. But in our opinion this demand can never be satisfied in practice without controlling the local carrier oscillator. An expedient from this problem may be an incoherent sequence-estimation with an attenuation of past metrics, i.e., a processing

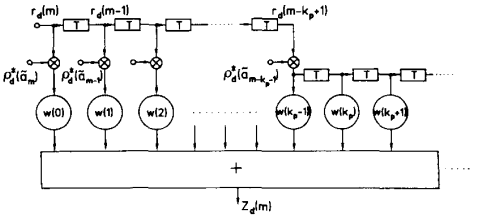

Fig. 10. Planar smoothing filter for the symbol-clock estimator with k_p parallel inputs.

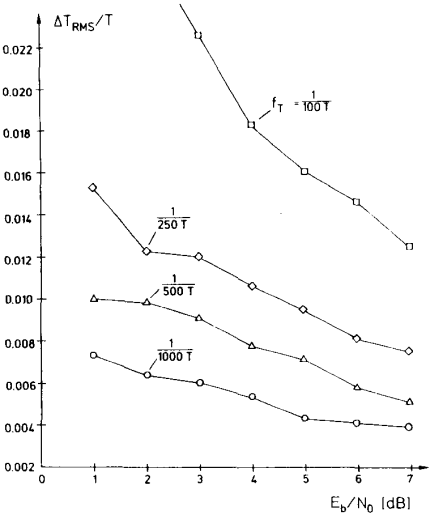

Fig. 11. Simulated RMS-deviation of the symbol-clock for different loop bandwidths f_T and perfect carrier-phase ($M = 4$, $h = 1/2$, 3RC, $D = 3$).

of the accumulated complex metrics by high-pass filters. But several tests have shown that for a cutoff-frequency of the metric high-pass filter, which is chosen sufficiently high for moderately fast phase variations, intolerable SNR-losses occur. Therefore, the coherent receiver structure together with an optimized synchronizer outperforms the incoherent sequence-estimation.

B. Symbol-Timing Synchronization

The simulation experiments have shown that the ML-estimate of the clock deviation was biased at a low SNR. This effect, which seriously interferes with time synchronization, is especially observable for partial response CPM schemes. A detailed analysis of this problem yields that the bias is caused by the special type of symbol errors within the sequence $\check{\boldsymbol{\alpha}}$ of preliminary estimated data, which occur when the path through the encoder-modulation trellis with the actually highest *a posteriori* probability changes. In such situations the sequence of signal elements $\rho(\check{\mathbf{a}}_i, t - iT)$, which corresponds to the preliminary estimated data violates the inherent trellis code of the CPM scheme, i.e., the phase continuity condition and the smoothing of the phase trajectories. These violations of the code cause unbalanced errors of the estimation of the symbol clock deviation.

In order to avoid the undesired bias, the total path through the trellis which actually has the highest probability has to be taken for the calculation of the components $Z_d(m)$ of the complex correlation. For simplification we propose a discrete time smoothing filter for the timing estimator with a small number k_p of parallel inputs; see Fig. 10. Only the vectors of the recent k_p signal elements associated with the path which actually has the best metric are fed into the smoothing filter. The simulation tests proved that at most five parallel inputs ($k_p \leq 5$) are sufficient for a total removal of the interfering bias, even at a very low SNR, where the estimated data have a high error rate. The parallel inputs require some additional complexity but do not reduce the speed of the estimator neither in a hardware nor in a software implementation. In Fig. 11 rms-values obtained by simulation of the (unbiased) steady-state deviations of the symbol-clock are given for several loop bandwidths f_T.

C. "Hang-Up"-Problem of the Joint Acquisition-Process

Unfortunately, for many CPM schemes with smoothed phase pulses ($L > 1$) "false locks" of the timing-synchronizer loop in wrong pseudo-stable positions may occur, when the joint synchronization process starts from a disadvantageous initial position. The reason for this fatal effect is the ex-

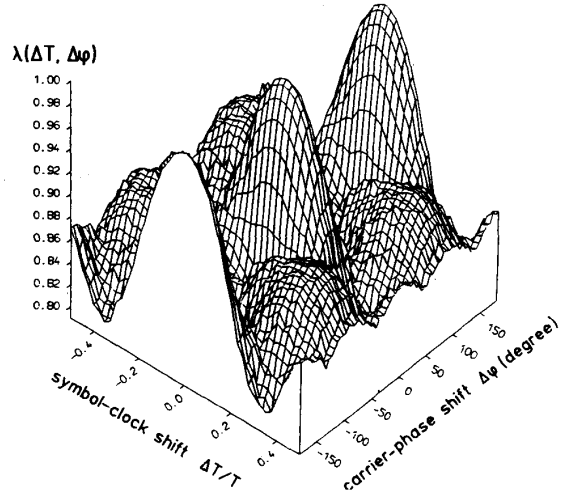

Fig. 12. Simulated likelihood-function (10). The estimated data sequence $\tilde{\alpha}$ is chosen in such a way that the maximum of (10) is achieved in each point, ($M = 4$, $h = 1/2$, 3RC, $D = 3$, no noise).

istence of second-order maxima in the likelihood-function $\lambda(\tilde{\alpha}, \Delta T, \Delta\varphi)$ [cf. (10)] for appropriate sequences $\tilde{\alpha}$ and pairs of clock shifts $\Delta T \neq 0$ and phase shifts $\Delta\varphi$ relative to the receiver-input signal, which do not correspond to one of the p possible steady-state positions. If the timing synchronizer tries to minimize the clock deviation by an adaptive approach, a "hang-up" of the process in such a second-order maximum cannot be avoided regardless of the applied estimator. In Fig. 12 this likelihood-function $\lambda(\tilde{\alpha}, \Delta T, \Delta\varphi)$ is shown for our special quaternary CPM scheme. At each point on the ΔT, $\Delta\varphi$-plane the maximum of the likelihood-function is selected over all data sequences $\tilde{\alpha}$ by a Viterbi-processor. Besides the first-order maxima at $\Delta T = 0$, $\Delta\varphi = 0°$ and $\Delta\varphi = \pm 180°$, which correspond to steady-state positions, four second-order maxima at $\Delta T = \pm T/3$, $\Delta\varphi = \pm 90°$ are evident. Therefore, the acquisition process, which starts from a worst case position, for example $\Delta T = 0.5T$ and $\Delta\varphi = 45°$ in Fig. 13, initially shows a "hang-up" in one of these pseudo-stable points. In Fig. 14 the likelihood-function for the same CPM scheme is shown once again, where for each fixed ΔT the maximum is selected over $\Delta\varphi$ and $\tilde{\alpha}$. These curves show that for a decreasing SNR the second-order maxima tend to disappear.

It is important to emphasize that the sequences $\tilde{\alpha}$ for which the likelihood-function attains the second-order maxima are quite different from the correct sequence α. Second-order maxima and hang-up problems were observed only for CPM schemes with smoothed phase pulses. For CPFSK schemes the joint acquisition of the steady-state position is no problem.

D. Proposals to Overcome the "Hang-Up"-Dilemma

Besides further possibilities we discuss three methods to overcome the "hang-up" dilemma of the symbol-timing synchronizer.

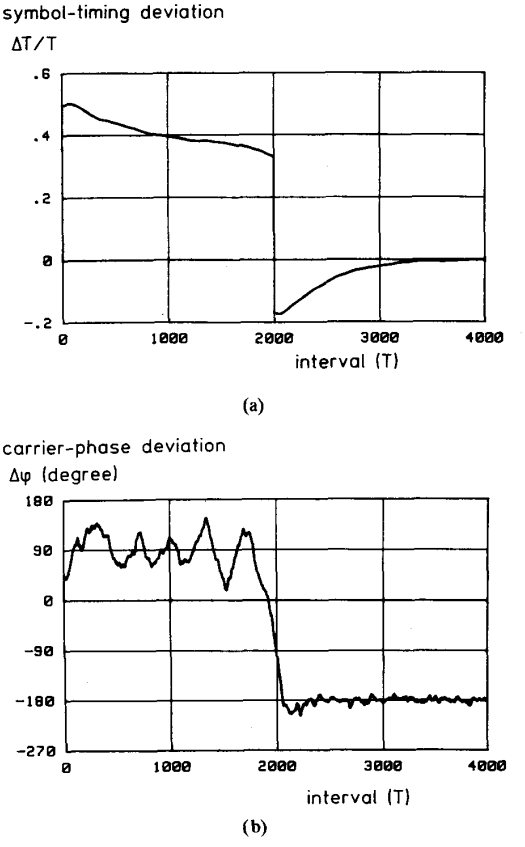

Fig. 13. Joint acquisition of the carrier-phase and the symbol-clock from a worst case initial position (A clock shift $\Delta T_s = -T/2$ is applied after detection of a "hang-up" event, receiver $D2$, $M = 4$, $h = 1/2$, 3RC, $D = 3$).

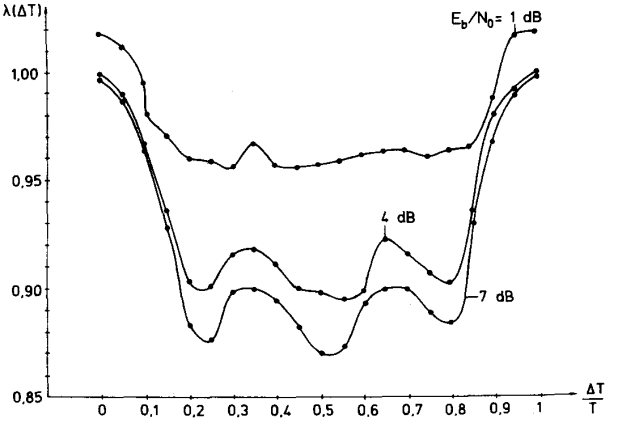

Fig. 14. Simulated likelihood-function (eq. 10). The data sequence $\tilde{\alpha}$ and the carrier-phase deviation $\Delta\hat{\varphi}$ are chosen in such a way that the maximum of (10) is achieved for each fixed ΔT ($M = 4$, $h = 1/2$, 3RC, $D = 3$).

D1) The adaptive approach using the gradient of the likelihood-function can be replaced by a parallel calculation of N complex correlations $Z_n(m)$ for different time shifts $n \cdot \Delta T_n$; $n \in \{0, 1, \cdots, N-1\}$, $\Delta T_N = T/N$, cf. [22]. Simply that time shift ΔT_n for which $Z_n(m)$ has the maximum

magnitude, is a quantized ML-estimate. But since different data sequences, which are fed back to the estimator, generate different maxima of the likelihood-function, it is not sufficient to calculate the $Z_n(m)$ for only one estimated data sequence $\tilde{\boldsymbol{\alpha}}$. In order to avoid a hang-up in any situation it is necessary to determine the particular optimum data sequences $\tilde{\boldsymbol{\alpha}}_n$ by N separate sequence estimators together with individual carrier-phase synchronizers. Therefore, the receiver using this direct approach exhibits a very high complexity.

D2) The difference of the likelihood-function between the first- and second-order maxima can be used for detection of a false-lock. In the receiver, the likelihood-function (11) is determined by a low-pass filter with a small bandwidth. A hang-up event is associated with a decrease of the filter output below a threshold, which has to be fixed between the first- and second-order maxima of the likelihood-function, cf. Fig. 12 and Fig. 14. The implementation of the hang-up detector is simple, as the likelihood-function is obtained as a byproduct of the carrier-phase estimator. A hang-up detection produces a certain time shift ΔT_S, (e.g., $T/2$ or $T/3$) of the local symbol-clock in order to push the tracking loop from the false-lock position. As soon as the new initial position lies within a propitious region of the $\Delta\varphi$, ΔT-plane, the steady state is immediately acquired. After such a time shift ΔT_S the hang-up detector should be inhibited for an interval T_{in}, which is necessary to achieve a stable point from the new initial position.

For a second-order timing loop with bandwidth f_T (Fig. 6), the simulations have shown that a cutoff frequency $f_{Tc} \approx f_T/2$ of a one-pole smoothing filter for the likelihood-function and an inhibition interval $T_{\text{in}} = 1/f_T$ are suitable parameters to minimize the average acquisition time. Various experiments for different CPM schemes verified the success of this method. In Fig. 13 after an inhibition interval of 2000 T the timing loop is pushed into a position from which a stable point is soon acquired.

In order to avoid clock shifts from the correct positions at a low SNR, the threshold of the hang-up detector has to be fixed very carefully (cf. Fig. 14) and a low cutoff frequency f_{Tc} has to be chosen. Therefore, this simple method suffers from a high inertia of the timing-loop and long acquisition times. Additionally, the hang-up detector is very sensitive to the gain of the receiver-input signal, because the likelihood-function has to be compared with an absolute threshold. Especially for time-variant channels this effect is a serious problem.

D3) Our third proposal to overcome the hang-up problem is a compromise between the structures $D1$ and $D2$. The receiver shown in Fig. 15 consists of three parallel sequence-estimation units together with independent carrier-phase synchronizers for the deviations $\Delta T_1 = 0$, $\Delta T_2 = T/3$, $\Delta T_3 = 2T/3$ of the actual symbol-clock. For each sequence-estimation unit, likelihood-functions $\lambda_n(m, \Delta T_n, \Delta\varphi_n(m))$ are calculated in the same way as described for the structure $D2$. In contrast to the structure $D1$, the local VCC is controlled by the output of the timing estimator of that sequence-estimation unit, which actually has the maximal likelihood-function (master). The output-data of the actual master are delivered to the sink. In order to avoid fast switching, a short inhibition time T_{in} is applied after a change of the master.

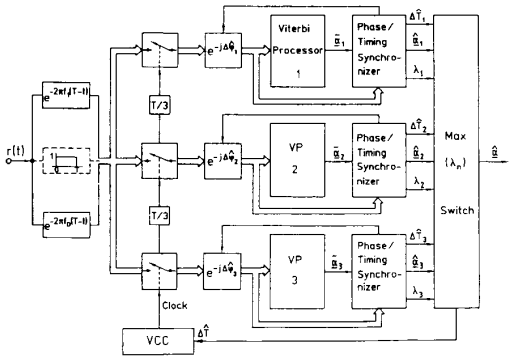

Fig. 15. Block diagram of a receiver involving three sequence estimation units with three independent carrier-phase estimators for a fast acquisition.

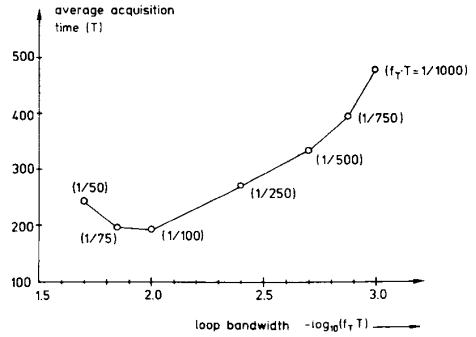

Fig. 16. Average time of the joint acquisition of the carrier-phase and symbol clock versus the bandwidth f_T of the symbol-timing loop, (simulation results with the receiver $D3$, $M = 4$, $h = 1/2$, 3RC, $D = 3$, $E_b/N_0 = 7$ dB, $f_\varphi = 1/(50\ T)$, $T_{\text{in}} = 50\ T$).

For many $M > 2$-ary CPM schemes with smoothed phase pulses the likelihood-functions are similar to that shown in Fig. 14. Thus, one of the three parallel sequence-estimator units always works with a symbol-clock which is close to the correct position and, therefore, the steady state is quickly acquired. As the actual master is selected by a comparison of likelihood-functions, this structure is insensitive to the gain of the receiver input signal.

In Fig. 16 the average time of the joint acquisition of the carrier-phase and the symbol-clock from 100 random initial positions is shown for this receiver structure. The acquisition of the steady state is defined by a residual timing error less than 0.06 T within at least 100 consecutive intervals. (The increase in the acquisition time for a high loop-bandwidth f_T is due to this restrictive definition, which is often violated in the steady state.) In Fig. 17 a final example of a joint acquisition process starting from a worst case initial position is given. Additionally, a high frequency-offset $\Delta f_c = 1/(10T)$ (36° per interval) of the local carrier-oscillator is applied. After an equalization of the frequency offset by the integrator of the carrier-phase loop, [Fig. 6(b)], the steady-state position is achieved in a fast process. This example and many further experiments show that the proposed data-aided synchronizer structures guarantee a secure acquisition even in extreme situations.

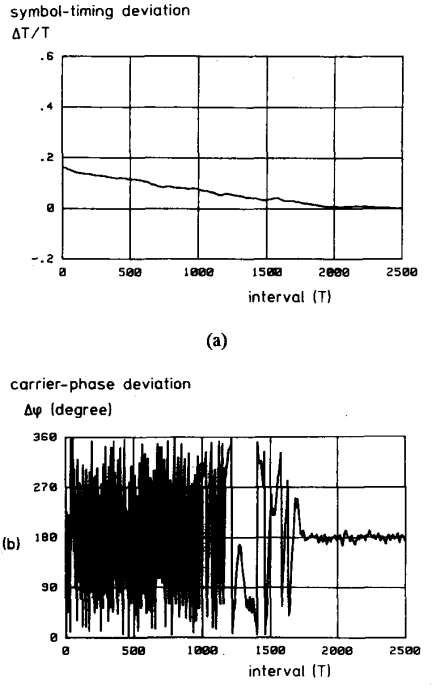

Fig. 17. Example of a joint acquisition process in the presence of a carrier frequency offset $1/(10\ T)$ (receiver $D3$, $M = 4$, $h = 1/2$, 3RC, $D = 3$, $f_\varphi = 1/(20\ T)$, $f_T = 1/(500\ T)$, $E_b/N_0 = 7$ dB).

V. Conclusion

The representation of signals in a signal space, which is formed by a few time-limited exponential basis-functions offers important advantages for coherent CPM receivers because simple explicit expressions exist for a data-aided ML-estimation of a deviation of the local symbol-clock relative to the receiver-input signal. Therefore, simple joint ML-estimators for carrier-phase and the symbol-timing can be derived. The hang-up problem of symbol-timing tracking loops was discussed. This effect is not a consequence of a special estimator but rather a natural property of CPM signals with smoothed phase pulses. Several solutions are proposed to overcome this problem.

The data-aided ML-esimators for the symbol-clock deviation and the joint estimators, which were derived in this paper for CPM, can also be applied to all kinds of digital transmission schemes, e.g., M-QAM or M-PSK. Besides the receiver input filters which are matched to the digital pulses, additional filters are necessary to generate spectral samples. But for some applications we think that these filters cause less expense than the calculation of the derivative of a ML-function [18] or a multiple implementation of detectors and/or decoders [21].

Acknowledgment

The authors are greatly indebted to the editor and the anonymous reviewers for valuable criticisms and suggestions.

References

[1] F. de Jager and C. E. Dekker, "Tamed frequency modulation, a novel method to achieve spectrum economy in digital transmission," *IEEE Trans. Commun.*, vol. COM-26, pp. 534–542, May 1978.
[2] T. Aulin, C.-E. Sundberg, and N. Rydberg, "Continuous phase modulation, Part I and II," *IEEE Trans. Commun.*, vol. COM-29, pp. 196–225, Mar. 1981.
[3] C.-E. Sundberg, "Continuous phase modulation," *IEEE Commun. Mag.*, vol. 24, no. 4, pp. 25–38, Apr. 1986.
[4] J. B. Anderson, T. Aulin, and C.-E. Sundberg, *Digital Phase Modulation.* New York: Plenum, 1986.
[5] J. G. Proakis, *Digital Communication.* New York: McGraw-Hill, 1989, 2nd ed.
[6] T. Aulin, C.-E. Sundberg, and A. Svensson, "MSK-type receivers for partial response continuous phase modulation," *ICC'82, Conf. Rec.*, Philadelphia, PA, June 1982, pp. 6F5.1–6F5.6.
[7] G. D. Forney, "The Viterbi algorithm," *Proc. IEEE*, vol. 61, pp. 268–278, Mar. 1973.
[8] T. Aulin and C.-E. Sundberg, "Synchronization properties of continuous phase modulation," *GLOBECOM'82, Conf. Rec.*, Miami, FL, Nov. 1982, pp. D7.1.1–D7.1.7.
[9] A. Premji and D. P. Taylor, "Receiver structures for multi-h signaling formats," *IEEE Trans. Commun.*, vol. COM-35, pp. 439–451, Apr. 1987.
[10] ——, "A practical receiver structure for multi-h CPM," *IEEE Trans. Commun.*, vol. COM-35, pp. 901–908, Sept. 1987.
[11] J. B. Anderson and D. P. Taylor, "A bandwidth-efficient class of signal space codes," *IEEE Trans. Inform. Theory*, vol. IT-24, pp. 703–712, Nov. 1978.
[12] J. Huber and W. L. Liu, "An alternative approach to reduced-complexity CPM-receivers," *IEEE J. Select. Areas Commun.*, vol. SAC-7, pp. 1437–1449, Dec. 1989.
[13] M. V. Eyuboglu and S. U. Qureshi, "Reduced-state sequence estimation with set partitioning and decision feedback," *GLOBECOM'86, Conf. Rec.*, Houston, TX, 1986, pp. 29.2.1–29.2.6.
[14] ——, "Reduced-state sequence estimation with set partitioning and decision feedback," *IEEE Trans. Commun.*, vol. 36, pp. 13–20, Jan. 1988.
[15] W. L. Liu, "Complexity reduction of coherent receivers for digital continuous phase modulation," Ph.D. dissertation, Inst. Commun. Eng., Univ. Fed. Armed Forces, Munich, FRG, May 1990.
[16] B. E. Rimoldi, "A decomposition approach to CPM," *IEEE Trans. Inform. Theory*, vol. IT-34, pp. 260–270, Mar. 1988.
[17] J. Huber and W. L. Liu, "Complexity reduction for coherent CPM receivers," *ITG Fachberichte 107, Conf. Rec.*, Nürnberg, FRG, 1989, pp. 219–224.
[18] L. E. Franks, "Carrier and bit synchronization in data communication—A tutorial review," *IEEE Trans. Commun.*, vol. COM-28, pp. 1107–1121, Aug. 1980.
[19] L. Hanbückers, "Nachrichtentechnische Grundlagen zur Optimierung eines CPM-Empfängers," Diplomarbeit, Univ. Fed. Armed Forces, Munich, FRG, Dec. 1989.
[20] T. Aulin and T. Larsson, "Two classes of algorithms for asymptotically optimal simplified MLSD with application of digital radio," *EUROCOM'88, Conf. Rec.*, Stockholm, Sweden, 1988, pp. 110–113.
[21] H. Meyr, "Signal processing in digital receivers: Model, algorithm, architecture," *ITG'89, Conf. Rec.*, Nürnberg, FRG, 1989, pp. 325–337.
[22] G. Ascheid and H. Meyr, "Maximum likelihood detection and synchronization by parallel digital signal processing," *GLOBECOM'84, Conf. Rec.*, pp. 32.2.1–32.2.5, 1984.
[23] A. Aghamohammadi, H. Meyr, and G. Ascheid, "Adaptive synchronization and channel estimation using extended Kalman filter," *IEEE Trans. Commun.*, vol. COM-37, pp. 1212–1219, Nov. 1989.
[24] P. Y. Kam, "Maximum-likelihood carrier phase recovery for linear suppressed-carrier digital data modulations," *IEEE Trans. Commun.*, vol. COM-34, pp. 522–527, June 1986.
[25] H. Kobayashi, "Simultaneous adaptive estimation and decision algorithm for carrier modulated data transmission systems," *IEEE Trans. Commun.*, vol. COM-19, pp. 268–280, June 1971.
[26] J. Huber and W. L. Liu, "Symboltakt- und Trägerphasensynchronisation für Kohärente Digitalsignalempfänger mit Mehrdimensionaler Signalrepräsentation," German Patent Application, no. P39 03 944.7, Feb. 13, 1989.
[27] ——, "Concatenation of RS-Code and CPM," *ISSSE'89, Conf. Rec.*, Erlangen, FRG, Sept. 1989, pp. 272–275.
[28] T. Andersson and A. Svesson, "Noncoherent detection of convolutionally encoded continuous phase modulation," *IEEE J. Select. Areas Commun.*, vol. SAC-7, pp. 1402–1414, Dec. 1989.

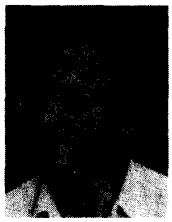

Johannes Huber (M'87) was born in Hausham, Bavaria, Federal Republic of Germany, in 1951. He received the Dipl.-Ing. degree in electrical engineering from the Technical University, Munich in 1977. From 1977 to 1982 he was a Research Assistant at the Institute for Communication Engineering of the University of the Federal Armed Forces, Munich, from which he received the Dr.-Ing. degree with a thesis on coding for channels with memory.

From 1982 to 1991, he was as Assistant Professor at the University of the Federal Armed Forces, Munich. In 1991 he was Visiting Scientist at the IBM Research Laboratory, Zurich, Switzerland. Since autumn 1991, he has been a full Professor at the University of Erlangen-Nuremberg, Germany. His research interests are coding theory, modulation schemes, high rate baseband transmission and algorithms for signal detection and adaptive equalization for channels with severe intersymbol interference. In 1988, he received the research award from the Deutsche Informationstechnische Gesellschaft.

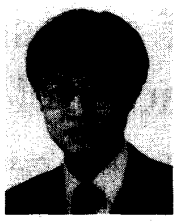

Weilin Liu (S'87) was born in Shanghai, People's Republic of China, on December 18, 1959. He received the Dipl.-Ing. degree in electrical engineering from the Technical University, Munich, Federal Republic of Germany, in 1986. Since October 1986 he has been a Research Assistant at the Institute for Communication Engineering of the University of the Federal Armed Forces, Munich, from which he received the Dr.-Ing. degree in May 1990.

Since April 1991 he has been with the Radio Systems Research Department of Ascom Tech. Ltd., Switzerland. His research interests include coding, modulation, signal detection and synchronization.